

1 Evolution of Anemone AR NOAA 10798 and the 2 Related Geo-Effective Flares and CMEs

Ayumi Asai,^{1,2,3} Kazunari Shibata,⁴ Takako T. Ishii,⁴ Mitsuo Oka,^{4,5} Ryuho

Kataoka,^{6,7} Ken'ichi Fujiki,⁷ and Nat Gopalswamy⁸

arXiv:0812.2063v1 [astro-ph] 11 Dec 2008

A. Asai, Nobeyama Solar Radio Observatory, National Astronomical Observatory of Japan,
Minamimaki, Minamisaku, Nagano, 384-1305, Japan. (asai@nro.nao.ac.jp)

¹ Nobeyama Solar Radio Observatory,

Abstract. We present a detailed examination of the features of the Active Region (AR) NOAA 10798. This AR generated coronal mass ejections (CMEs) that caused a large geomagnetic storm on 24 August 2005 with the minimum Dst index of -216 nT. We examined the evolution of the AR and the features on/near the solar surface and in the interplanetary space. The AR emerged in the middle of a small coronal hole, and formed a *sea anemone* like configuration. $H\alpha$ filaments were formed in the AR, which have southward axial field. Three M-class flares were generated, and the first two that occurred on 22 August 2005 were followed by Halo-type CMEs. The speeds of the CMEs were fast, and recorded about 1200 and 2400 km s^{-1} , respectively. The second CME was especially fast, and caught up and interacted with the first (slower) CME during their travelings toward Earth. These acted synergically to generate an interplanetary disturbance with strong southward magnetic field of about -50 nT, which was followed by the large geomagnetic storm. *Accepted for publication in JGR. Copyright (2008) American Geophysical Union. Further reproduction or electronic distribution is not permitted.*

National Astronomical Observatory of

1. Introduction

Space weather has attracted a lot of attention in recent times. Space weather research involves various related fields, such as the solar surface, solar wind, interplanetary space, geomagnetosphere, ionosphere, and atmosphere, since a comprehensive understandings from active phenomena on the solar surface to the propagation of the disturbances toward Earth are crucially required for the studies.

Vast plasma ejected from the solar corona in the form of coronal mass ejections (CMEs) leads to a geomagnetic storm, and therefore, CMEs have been actively discussed. Moreover, large geomagnetic storms are associated with large flares (that are emitting strong X-ray), long duration events (LDEs), fast CMEs, and so on (e.g., Gopalswamy, Yashiro, & Akiyama 2007). Flare locations are another factor for a major geomagnetic storm, since the flare location close to the disk center indicates that the related CME is heading towards Earth and is likely to cause a large geomagnetic storm (Manoharan et al. 2004). Ejections that cause strong disturbances with southward magnetic field in the interplanetary space are also important. Coronal holes (CHs) are, on the other hand, related with fast solar wind because of their open magnetic field, and therefore, themselves have been another important factor for space weather studies. While large geomagnetic storms are caused by earth-directed CMEs (see e.g., Gosling et al. 1990), weaker storms are associated with high-speed streams from CHs (see e.g., Sheeley, Harvey, & Feldman 1976). However, storms related to high-speed streams from CHs cause larger flux enhancement of MeV electrons of the Earth's Van Allen belt than the CME-associated storms do on

Japan, Minamimaki, Minamisaku, Nagano,

average (Kataoka & Miyoshi 2006). It has been, furthermore, reported that many fast Halo CMEs are associated with CHs (Verma 1998; Liu & Hayashi 2006). The recent work done by Liu (2007) showed that the speeds are faster even statistically than those of CMEs under the heliospheric current sheet. Therefore, in order to understand what kind of events can generate a large geomagnetic storm, it is necessary to study active phenomena on the solar surface and the propagation in the interplanetary space, in relation to the surrounding magnetic structure.

In this paper we examine in detail the evolution of an Active Region (AR) that emerged in a CH and the related flares, CMEs, and the geomagnetic storm to elucidate how such a magnetic configuration works to generate a geo-effective flares/CMEs. CMEs originating from AR NOAA 10798, generated a large geomagnetic storm on 24 August 2005, which was one of the 88 major geomagnetic storms reported by Zhang et al. (2007). This AR has been highly paid attention to, since it was one of the targets of the International CAWSES¹ Campaign², and at the related virtual conference³, there were intensive discussions on the AR (e.g., Asai et al. 2006). Figure 1 shows an overview of the geomagnetic storm and the related solar-terrestrial events. The Soft X-ray (SXR) flux in the *GOES* 1.0 - 8.0 Å channel shows three M-class flares that occurred on 22 and 23 August 2005. The first two flares (marked with ×) were associated with the CMEs responsible for the geomagnetic storm in question. In the second panel we can recognize the sufficient enhancements of the proton fluxes in >10 MeV (black line) and >50 MeV (gray line) channels obtained with *GOES*. Both flares were followed by enhancements of solar energetic particles (SEPs), and the second flare's was larger. The bulk velocity of solar wind V_{sw} in the third panel

384-1305, Japan.

62 and the total $|B|$ (black line) and Z-component of the magnetic field B_z (gray line) in the
 63 fourth panel were measured with the *Advanced Composition Explorer* (ACE). The first

² National Astronomical Observatory of
 Japan, Minamimaki, Osawa, Mitaka, Tokyo,
 181-8588, Japan.

³ The Graduate University for Advanced
 Studies (SOKENDAI), Japan.

⁴ Kwasan and Hida Observatories, Kyoto
 University, Yamashina, Kyoto, 607-8471,
 Japan.

⁵ Center for Space Plasma and Aeronomic
 Research, University of Alabama in
 Huntsville, AL 35805, USA.

⁶ RIKEN (The Institute of Physics and
 Chemical Research), 2-1 Hirosawa, Wako,
 Saitama, 351-0198 Japan.

⁷ Solar-Terrestrial Environment
 Laboratory Nagoya University, Chikusa,
 Nagoya, Aichi, 464-8601, Japan.

⁸ NASA Goddard Space Flight Center,
 Greenbelt, MD 20771, USA.

shock was recorded at 05:35 UT by *ACE* as shown by the dashed line. The same shock was also recorded by the *Geotail* satellite at 06:15 UT. The interplanetary magnetic field had a strong southward component of about -50 nT. The bottom panel shows the Dst index produced by the Kyoto University. The decrease of the Dst index was quite large, reaching -216 nT. In §2 we describe the evolution of the AR, focusing on the photospheric magnetic configuration, and the $H\alpha$ filament formed during the evolution of the AR and the coronal features are also presented. In §3 we discuss the flares/CMEs that occurred on 22 August 2005. In §4 we shortly review the associated interplanetary disturbances. In §5 we summarize our results.

2. Evolution and Structure of Active Region NOAA 10798

2.1. Evolution

First, we examine the evolution of the photospheric magnetic field. Figure 2 shows the continuum images (top panels), the magnetograms (middle panels), and the extreme ultraviolet (EUV) images of AR 10798. The continuum images and the magnetograms were obtained with the Michelson Doppler Imager (MDI; Scherrer et al. 1995) aboard the *Solar and Heliospheric Observatory* (*SOHO*; Domingo, Fleck, and Poland 1995), while the EUV images are taken with the Extreme-Ultraviolet Imaging Telescope (EIT; Delaboudinière et al. 1995) aboard *SOHO*. Each image was taken at about 00:00 UT of the day. AR 10798 emerged on 18 August 2005 and rapidly evolved.

Although the region showed a simple bipolar configuration, while it was in violation of the so-called “Hale-Nicholson’s magnetic polarity law” (Hale et al. 1919), according to which the preceding spots in the southern hemisphere should have a negative polarity during solar cycle 23. These “reverted polarity” ARs are statistically more likely to

generate flares and CMEs (López Fuentes et al. 2003; Tian et al. 2005). We checked all the ARs that appeared in 2005, and found that only 7 ARs (5 %), including the AR 10798, were the “reverted polarity” ARs. Furthermore, 4 of the 7 ARs, including AR 10798, showed high solar activity. This implies that AR 10798 had potentially a very complex structure. For example, a highly twisted and kinked magnetic structure may be embedded beneath the photosphere as Ishii, Kurokawa, & Takeuchi (2000) and Kurokawa, Wang, & Ishii (2002) reported. Indeed, we can see the rotating motion of the pair of the sunspots counter-clockwise during the disk passage. This AR further evolved and generated an X17 flare on 7 September 2005 when it returned as NOAA 10808 (Wang et al. 2006, Nagashima et al. 2007).

The top panel of Figure 3 shows the SXR lightcurves obtained by *GOES* in the 1.0 – 8.0 Å (upper) and 0.5 – 4.0 Å (lower) channels. The bottom panel of Figure 3 shows the time profiles of the magnetic flux of this AR. That for the negative magnetic flux is multiplied by -1 . The calculated area is $400'' \times 400''$, and is as wide as it covers the whole AR. Following the emergence and evolution of the active region from 18 August 2005, the magnetic fluxes as well as the SXR intensity gradually increased, with three M-class flares occurring on 22 and 23 August, before rotating behind the west limb. In this paper we mainly discuss the first two flare that occurred on 22 August 2005, since the geomagnetic storm on 24 August 2005 is attributed to the related eruptions/CMEs.

2.2. Filament Formation

Second, we examine the filament formation in AR 10798, using the $H\alpha$ images. A filament is just a visualized part of a helical flux rope, and it is only a fraction of the whole of the flux rope. However, it is thought that it is located in the middle of the flux

rope, and that a filament even represents the whole structure (see e.g., Low & Hundhausen 1995). Therefore, an eruption of a filament is always related with a large scale disturbance of the coronal magnetic field that often appears as an EIT dimming. As Munro et al. (1979) suggested that more than 70% of CMEs are associated with eruptive prominences or filament disappearances (with or without flares), and therefore, filament eruptions are very important as a CME-associated phenomenon. Moreover, we often see an ejected filament observed in $H\alpha$ s/microwaves or a plasmoid in SXR at the center of an ejecta, when it is accompanied by a flare. We can even roughly extrapolate the magnetic configuration of a CME from that of the ejected filament. For example, Rust (1994) showed that the helicity of ejected filaments correspond to the chirality of magnetic clouds passing Earth (about 4 days after the eruptions).

Figure 4 shows the temporal evolution of the AR in the $H\alpha$ images (top panels) and the magnetic field (bottom panels). The $H\alpha$ images in Figure 4a and 4b were taken with the Solar Magnetic Activity Research Telescope (SMART⁴) at Hida Observatory, Kyoto University. Figure 4c and 4d were obtained at the Observatoire de Paris, Section de Meudon and the Big Bear Solar Observatory, respectively. Both of these images were obtained through the on-line data center of the Global High-Resolution $H\alpha$ Network⁵. The magnetograms (Fig. 4e - 4h) were taken by *SOHO*/MDI.

For three days after the emergence of the AR (until 20 August), a clear arch-filament system (Bruzek 1967) was seen (Fig. 4a). The bipole-like systems bridged the neutral line and connected the spots of opposite polarity. On the other hand, after 21 August 2005, these filamentary structure was abruptly changed. In Figure 4b, some oblique structure appeared, and showed pre-filamental structure. Comparing with the magnetograms (the

bottom panels of Figure 4), we confirm that the magnetic field of these structure was oriented from northwest to southeast, which means they had southward magnetic field. About nine hours after this (Fig. 4c), the sheared filamentary structure evolved to a large $H\alpha$ filament that lay on the magnetic neutral line between the sunspots. The arrow in Figure 4c points to the filament. The filament formation is consistent with what Martin (1973) pointed out long ago: developed filaments usually become apparent about the “fourth day” after the initial formation of an active region. Unfortunately, there are no data between Figure 4b to 4c, but we can see the new flux emergence around the magnetic neutral line, (compare Figure 4f with 4g). The formation of the filaments with the southward magnetic field is probably related to the emerging flux.

The first M-class flare occurred at 00:44 UT on 22 August 2005, which is in the middle of the time between Figure 4c and 4d. In Figure 4d, we can recognize the disappearance of the $H\alpha$ filament after the first flare, while a new filament formed in the south part of the AR as pointed by the arrow in the panel. Associated with the first flare, the $H\alpha$ filament formed in the northern part (Fig. 4c) erupted, and with the second flare, the southern one (Fig. 4d) erupted. The axial field of these filaments had southward magnetic field, which is easily inferred from the pre-filamentary structure. Although we also checked the EUV data taken with EIT and the Transition Region and Coronal Explorer, we could not find out any phenomena that can be a source of the CMEs other than the filament eruptions. We will discuss the flares and CMEs in more detail in §3.

2.3. Anemone Structure

Figures 5a,b show the coronal structure of the AR observed at about 00:00 UT on 20 August 2005, in SXR and in EUV with Solar X-ray Imager (SXI) on board *GOES* and

SOHO/EIT, respectively. The bright structure near the center of the image is AR 10798. Figure 5c shows the magnetogram taken by *SOHO*/MDI. The following sunspot with the negative (that is *black*) polarity is the center of the EUV bright structure, and a radial array of loops is formed. We also present schematic cartoons of the magnetic structure of AR 10798 in Figure 6a and b.

The appearance is like a *sea anemone*, and this type of ARs is sometimes called “anemone structure” (Shibata et al. 1994a, 1994b), or originally “fountain” (Tousey et al. 1973, Sheeley et al. 1975a) in the *Skylab* era. We call these ARs “anemone ARs” in this paper. These anemone ARs are often associated with the emerging fluxes within unipolar regions (Sheeley et al. 1975b), and in most cases, they appear in CHs (Asai et al. 2008). Although characteristics of anemone ARs have been mainly discussed only in SXR, they are commonly seen under such a magnetic configuration, even in a chromospheric line by the Solar Optical Telescope on board *Hinode* (Shibata et al. 2007).

As shown in Figure 5, AR NOAA 10798 is clearly surrounded with a unipolar region with the positive magnetic polarity, and shows the anemone appearance both in SXR and in EUV, and we can conclude that NOAA 10798 was a typical anemone AR. In emerging, the AR interacted (reconnected) with the ambient coronal field, and magnetic loops were arranged radially with the following spot that has the negative magnetic polarity as the center of the anemone structure. In Figure 5b the dark region surrounding the AR is a CH. On 22 August, when the flares/CMES in the matter occurred, the anemone appearance somewhat changes as seen in Figure 2. This is caused by projection like many anemone ARs, while some anemone ARs keep the appearance even on the limb (Saito et al. 2000).

3. Flares and CMEs

Next, we focus on the two M-class flares and the associated CMEs. The first flare that was M2.6 on the *GOES* scale, started at 00:44 UT, and peaked at 01:33 UT. The second one was M5.6 on the *GOES* scale, and the start and the peak times were 16:46 UT and 17:27 UT, respectively. Both are LDEs, and showed clear arcade structure. Figure 6c shows a schematic of the magnetic field during the flares. The sites of the flares were (S11° W54°) and (S12° W60°), respectively.

The two flares were associated with disappearances of the H α filaments, and Halo-type CMEs that were observed with the Large Angle Spectrometric Coronagraph (LASCO) aboard *SOHO* (see the *SOHO*/LASCO CME online catalog⁶; Yashiro et al. 2004). LASCO images of the two CMEs (CME1 and CME2) are shown in Figure 7. The left panels are the LASCO C2 running difference images overlaid with EUV images taken by *SOHO*/EIT (195Å), and the right panels are the LASCO C3 running difference images. CME1 was ejected mainly to the northwest, and CME2 was to the southwest as indicated by the arrows in Figure 7. The directions were roughly consistent with the initial position of the H α filaments (see, §2.2).

It is particularly notable that the CMEs were quite fast: CME1 and CME2 had speeds of about 1200 and 2400 km s⁻¹, respectively. The speed of CME2 is ranked among the top 17 of all the 13,000 CMEs observed by *SOHO*/LASCO until the end of 2007. Although the time interval between the two flares/CMEs was about 16 hours, CME2 possibly caught up with CME1 before reaching 1 AU (Gopalswamy et al. 2001a). Statistically, a CME ejected with the velocity of V_{CME} have an acceleration $a \text{ m s}^{-2} = 2.193 - 0.0054 \times V_{\text{CME}}$ km s⁻¹ (Gopalswamy et al. 2001b), and the expected accelerations for CME1 and CME2

are -4.3 and -10.8 m s^{-1} for the current case. Therefore, we estimate that the interacting
between CME1 and CME2 occurred at about 1 AU (i.e. near Earth), by assuming constant
accelerations for the CMEs.

The interplanetary disturbance associated with the Halo-type CMEs can be followed by
using interplanetary scintillation (IPS). When we see a radio source through a highly tur-
bulent plasma associated with a CME traveling from the Sun, the radio source scintillates.
Therefore, such scintillations show us the the electron density fluctuation caused by the
CME. As an effective indicator of the electron density fluctuation, we often use g-value
(g) calculated from IPS data (see Tokumaru et al. 2000, 2003, 2005 for more details).
The g-value represents the variation of the electron density fluctuation in the solar wind
(ΔN_e), as $g^2 \propto \int_0^\infty \Delta N_e^2 w(z) dz$, where z is a distance along the line-of-sight, and $w(z)$
is the IPS weighting function given by Young (1971). It is normalized to the mean level
of density fluctuations so that the quiet solar wind yields g-value around unity, and the
enhancement ($g > 1$) shows the passing of a turbulent plasma.

We examined the g-values taken with IPS at Solar-Terrestrial Environment Laboratory
(STEL), Nagoya University (Kojima & Kakinuma 1990, Asai et al. 1995, Tokumaru
et al. 2000). Figure 8 shows the daily (Japanese daytime) sky projection maps of the
g-values. In each map, the center corresponds to the location of the Sun, and dotted
cocentric circles are constant radii contours from the Sun drawn at 0.3, 0.6, and 0.9 AU.
The solid circles indicate the points of the closest approach to the Sun (P-points) on
the line-of-sight where g-value were obtained (P-point approximation). The locations of
the stronger g-values are emphasized by colors and sizes of the circles. The dark gray
and the black circles represent the locations where the g-values are larger than 1.5 and

2.0, respectively. In the both panels of Figure 8 we can see density fluctuations that were caused by the two Halo CMEs, while we cannot distinguish the individual CMEs discretely due the low spatial resolution of IPS. The front of the disturbance, which was caused by CME1, reached about 0.4 and 0.8 AU on August 23 and 24, respectively. CME1 is well decelerated, and the speed is about 700 km s^{-1} . These fluctuations are distributed roughly in all direction.

4. Interplanetary Disturbance

Here, we investigate in more detail why a strong disturbance with a magnetic field of about -50 nT arrived at Earth. As we mentioned above (see §4), CME2 probably caught up with CME1, and therefore, disturbance is regarded as a merged product of CME1 and CME2, although the interaction was not directly observed.

Figure 9 shows a 7-hour interval corresponding to the geo-effective part of the interplanetary disturbance from *Geotail*. The top four panels present the magnetic field in GSE coordinates obtained by the magnetic-field experiment (MGF; Kokubun et al. 1994). The magnitude $|B|$ and the x- (B_x), y- (B_y), and z-components (B_z) of the magnetic field are shown. The fifth panel shows the ion velocity V_x observed with the low energy particle experiment (LEP; Mukai et al. 1994). The bottom panel shows the electron density N_e observed by the plasma wave instrument (PWI; Matsumoto et al. 1994). The density reached so high that the counts of the particle detectors onboard *Geotail* (and probably *ACE* as well) were saturated, and therefore, it is underestimated during the strong disturbance. To avoid the underestimation of the density, we simply traced local enhancements of the electrostatic noise that appears in the dynamic spectra of the electric field as have been carried out elsewhere (see e.g., Fig. 4 of Terasawa et al., 2005). Al-

though the measurement also have a uncertainty, it is more accurate than that by particle measurement experiments, since the counts were not saturated.

A flux rope (FR) structure can be identified by the smooth rotation of the magnetic field from 09:15 to 11:15 UT as shown by the vertical dashed lines in Figure 9. It is notable that the 2 hours duration of this FR was extremely short compared to the typical duration of about 20 hours (Lepping et al. 2003; Gopalswamy 2006). The local velocities of the FR is 650 km s^{-1} , as will be discussed below. We estimated the radial size of the FR to be about 0.03 AU, by multiplying the local velocity by the 2 hours duration. This value is also extremely small compared with typical ones of 0.2 - 0.3 AU (Forsyth et al. 2006). This FR showed the smooth rotation from positive to negative B_y , a negative B_z peak in the middle of the B_y rotation, and relatively small B_x component. These can be roughly explained by the passage of a right-handed flux rope with the southward pointing axis field, which is consistent with the magnetic field configuration of the associated H α filaments. The largest geomagnetic storm of cycle 23 that occurred on 20 November 2003 was associated with a similar FR (Gopalswamy et al. 2005).

About 15 minutes before the front edge of the FR (i.e. at about 09:00 UT), a solar wind discontinuity is identified by the sudden increases in the magnetic field, solar wind speed, and density as shown by the vertical solid line. From the variation of velocity distribution function, we confirmed an abrupt increase of temperature (not shown) there, and concluded that the discontinuity is a shock. We call the discontinuity as the “second shock”, and the “first shock” is for the one observed at the beginning of the event as shown with the dashed line in Figure 1 and the vertical solid line at about 06:15 UT in Figure 9.

The extremely strong southward magnetic field, the unusual short duration of the FR (2 hours), and very small separation between the second shock and the FR front (15 minutes) can be naturally explained, if we regard the disturbance as the product of very fast shock wave associated with CME2 interacting with the slower body of CME1 in traveling to Earth. Therefore, CME2 suffered from a strong deceleration, which implies that there was a great compression of the interplanetary medium in front of CME2. In this case the first and the second shocks are thought to be associated with CME1 and CME2, respectively.

The local velocities of the first and the second shocks are measured by the positional relation between the *ACE* and *Geotail* satellites, and therefore, we can roughly estimate their accelerations (decelerations). *ACE* and *Geotail* were located at (223.7, 10.6, 4.5) and (12.9, 25.7, 1.9) R_E ($= 6378$ km) at 09:00 UT on 24 August 2005 in GSE coordinate system, respectively. As already mentioned, CME1 and CME2 were ejected with velocities of about 1200 and 2400 km s^{-1} , at intervals of 16 hours. On the other hand, the local velocities of the first and the second shocks are 650 and 710 km s^{-1} , respectively, and the time separation between them is reduced to only about 3 hours. Assuming the constant accelerations, they are estimated to be -3.2 and -13 m s^{-2} . As we calculated above, the accelerations for CME1 and CME2 are statistically expected to be -4.3 and -10.8 m s^{-1} . The additional deceleration of CME2 also indicates that it interacted with slower CME1 and compressed the interplanetary medium there.

5. Summary and Discussions

In order to make clear the importance of an AR that emerged in a CH to generate geo-effective flares/CMES, we examined the evolution of the AR NOAA 10798, the solar events

associated with a geomagnetic storm that occurred on 24 August 2005, and the related interplanetary disturbances. The summary of the features of the AR and the events is as follows: (1) Highly twisted and complex magnetic flux emerged within a small CH on 18 August 2005, which was named NOAA 10798, (2) An anemone type structure was generated, and $H\alpha$ filaments that had southward axial fields were formed on 21 August 2005, (3) Two halo CMEs associated with M-class flares occurred on 22 August 2005. (4) The CME speeds were fast, especially the second one recorded 2400 km s^{-1} , (5) The interplanetary disturbances with strong southward magnetic field of about -50 nT and strong compression of plasma were produced.

The CMEs were particularly geo-effective, and the minimum Dst index was -216 nT . The reasons for the CMEs to be so geo-effective were the high speeds of the two CMEs and their interaction as well as the CMEs traveled directly toward the earth. For the current case, the speed of CME2 was faster and pushed the slower CME1, which led to a unusual strong compression of the plasma at the front of CME2.

The high speeds of the CMEs are more notable. The AR was large and very complex, and violated the Hale-Nicholson's magnetic polarity law. These reverted polarity ARs are statistically favorable to produce large flares. However, it is suspicious whether just the violation of the Hale-Nicholson's law is responsible for high speed CMEs of about 2000 km s^{-1} , and it should be quantitatively and statistically clarified in the future. In this paper we suggest that the fast CMEs are probably a consequence of the eruption inside a CH from an anemone AR. This is consistent with the association between fast Halo CMEs and CHs as reported before (Verma 1998; Liu & Hayashi 2006; Liu 2007).

Eruptive activities of anemone ARs are usually low (Asai et al. 2008), and often confined to small-scale activities inside CHs that appears to be SXR bright points. In some cases, anemone ARs can produce large SXR coronal jets (Shibata et al. 1994b, Vourlidas et al. 1996, Kundu et al. 1999, Alexander & Fletcher 1999). This is because the situation of an emergence of a magnetic flux within a CH is suitable for magnetic reconnection with the surrounding field to generate SXR coronal jets and/or $H\alpha$ surges (Yokoyama & Shibata 1995, 1996). Wang (1998) indicates the possibility that even polar plumes are associated with jets from anemone ARs at high latitudes. Anemone ARs are related to non-radial coronal streamers emanating from magnetically high latitudes (Saito et al. 2000). The relation between anemone ARs and fast solar winds have also been paid attentions to (Takahashi et al. 1994, Saito et al. 1994, Wang 1998). Saito et al. (2000) further discussed the rotational reversing model and the triple dipole model to explain the reversal of the solar surface magnetic field, and anemone ARs play an important role in this. This model implies that anemone ARs are more conspicuous in the decaying phase of a solar cycle as in the case of AR NOAA 10798.

On the other hand, the deflection of CMEs eastward by the interplanetary fields effectively worked in the current case as shown in the Figure 6d. As Wang et al. (2004) pointed, the faster CMEs are deflected more eastward, and therefore, the AR NOAA 10798 generated geo-effective CMEs, although it was quite close to the southwest limb. The azimuthal angle of the magnetic field measured from the x-axis $\phi_B (= \arctan(B_y/B_x))$ changed $90^\circ - 180^\circ - 270^\circ (-90^\circ)$ during the passage of the FR, which is consistent with the guess that the deflection of the CMEs were so strong that the axis of the FR passed through the east of the earth. This is also consistent with the fact that the flares in the

next rotation (and renamed as NOAA 10808) did not affect the magnetosphere so much (Wang et al. 2006, Nagashima et al. 2007). Furthermore, the extremely short duration of FR and the missing of CME1 (see Fig. 9) are possibly explained by the skimming encounter with the CMEs due to the strong deflection.

The nature of the interplanetary disturbances and their impact on the magnetosphere strongly depend on the features of emergence and evolution of an AR and the relation with the surrounding magnetic field. In this work we succeeded to follow in detail the evolution of the AR and the large geomagnetic storm resulting from eruptions in the AR. The reconstruction of the proposed scenario using numerical simulations will be attempted in the future.

Acknowledgments. This work was supported by the Grant-in-Aid for the Global COE Program “The Next Generation of Physics, Spun from Universality and Emergence” from the Ministry of Education, Culture, Sports, Science and Technology (MEXT) of Japan. This work was also supported by the Grant-in-Aid for Creative Scientific Research “The Basic Study of Space Weather Prediction” (17GS0208, Head Investigator: K. Shibata) from the Ministry of Education, Science, Sports, Technology, and Culture of Japan. This work was partially carried out by the joint research program of the Solar-Terrestrial Environment Laboratory, Nagoya University. We would like to acknowledge all the members of the *Geotail*/PWI, LEP, and MGF for providing the data. We would like to thank WDC for Geomagnetism, Kyoto Dst index service. Our thanks also go to the SMART teams of Hida Observatory, Kyoto University, Big Bear Solar Observatory, and Meudon Observatoire de Paris, Section de Meudon for letting us use the $H\alpha$ data. We made extensive

use of *SOHO*, and *ACE* Data Center. MO was supported by the Grant-in-Aid for JSPS
Postdoctoral Fellows for Research Abroad.

Notes

1. Climate And Weather of the Sun-Earth System
2. see, <http://www.bu.edu/cawses/secondcampaign.html>
3. <http://workshops.jhuapl.edu/s1/index.html>
4. <http://www.hida.kyoto-u.ac.jp/SMART/>
5. <http://www.bbso.njit.edu/Research/Halpha/>
6. http://cdaw.gsfc.nasa.gov/CME_list/

References

- Alexander, D., and Fletcher, L. (1999), High-resolution Observations of Plasma Jets in the Solar Corona, *Sol. Phys.*, *190*, 167, doi: 10.1023/A:1005213826793.
- Asai, A., K. Shibata, T. T. Ishii, N. Gopalswamy (2006), Anemone Structure of NOAA 10798 and Geo-Effective Flares/CMES, url: <http://workshops.jhuapl.edu/s1/conf/solar-wind/asai-01/asai-01.pdf>.
- Asai, A., K. Shibata, H. Hara, N. V. Nitta (2008), Characteristics of Anemone Active Regions Appearing in Coronal Holes Observed with *Yohkoh* Soft X-ray Telescope, *Astrophys. J.*, *673*, 1188, doi: 10.1086/523842.
- Asai, K., Y. Ishida, M. Kojima, K. Maruyama, H. Misawa, N. Yoshimi (1995), Multi-Station System for Solar Wind Observations Using the Interplanetary Scintillation Method, *J. Geomagn. Geoelectr.*, *47*, 1107.

- Bruzek, A. (1967), On Arch-Filament Systems in Spotgroups, *Sol. Phys.*, *2*, 451, doi: 10.1007/BF00146493.
- Delaboudinière, J.-P., et al. (1995), EIT: Extreme-Ultraviolet Imaging Telescope for the SOHO Mission, *Sol. Phys.*, *162*, 291, doi: 10.1007/BF00733432.
- Domingo, V., B. Fleck, A. I. Poland (1995), The SOHO Mission: an Overview, *Sol. Phys.*, *162*, 1, doi: 10.1007/BF00733425.
- Forsyth, R. J., et al. (2006), ICMEs in the inner heliosphere: origin, evolution and propagation effects, *Space Sci. Rev.*, *123*, 383, doi: 10.1007/s11214-006-9022-0.
- Gopalswamy, N., S. Yashiro, M. L. Kaiser, R. A. Howard, J.-L. Bougeret (2001a), Radio Signatures of Coronal Mass Ejection Interaction: Coronal Mass Ejection Cannibalism?, *Astrophys. J.*, *548*, L91, doi: 10.1086/318939.
- Gopalswamy, N., A. Lara, S. Yashiro, M. L. Kaiser, R. A. Howard, Russell (2001b), Predicting the 1-AU arrival times of coronal mass ejections, *J. Geophys. Res.*, *106*(A12), 29207, doi: 10.1029/2001JA000177.
- Gopalswamy, N., S. Yashiro, G. Michalek, H. Xie, R. P. Lepping, R. A. Howard (2005), Solar source of the largest geomagnetic storm of cycle 23 *Geophys. Res. Lett.*, *32*, L12S09, doi: 10.1029/2004GL021639.
- Gopalswamy, Nat (2006), Properties of Interplanetary Coronal Mass Ejections, *Space Sci. Rev.*, *124*, 145, doi: 10.1007/s11214-006-9102-1.
- Gopalswamy, N., S. Yashiro, S. Akiyama (2007), Geoeffectiveness of halo coronal mass ejections *J. Geophys. Res.*, *112*, A06112, doi: 10.1029/2006JA012149.
- Gosling, J. T., S. J. Bame, D. J. McComas, J. L. Phillips (1990), Coronal Mass Ejections and Large Geomagnetic Storms, *Geophys. Res. Lett.*, *17*, 901.

- 390 Hale, G. E., F. Ellerman, S. B. Nicholson, A. H. Joy (1919), The Magnetic Polarity of
391 Sun-Spots, *Astrophys. J.*, *49*, 153, doi: 10.1086/142452.
- 392 Ishii, Takako T., H. Kurokawa, T. T. Takeuchi (2000), Emergence of Twisted Magnetic-
393 Flux Bundles and Flare Activity in a Large Active Region, NOAA 4201, *PASJ*, *52*,
394 337.
- 395 Kataoka, R., and Y. Miyoshi (2006), Flux enhancement of radiation belt electrons during
396 geomagnetic storms driven by coronal mass ejections and corotating interaction regions,
397 *Space Weather*, *4*, S09004, doi: 10.1029/2005SW000211.
- 398 Kojima, M., T. Kakinuma (1990), Solar Cycle Dependence of Global Distribution of Solar
399 Wind Speed, *Space Sci. Rev.*, *53*, 173.
- 400 Kokubun, S., T. Yamamoto, M. H. Acuna, K. Hayashi, K. Shiokawa, and H. Kawano
401 (1994), The GEOTAIL magnetic-field experiment, *J. Geomagn. Geoelectr.*, *46*, 7.
- 402 Kurokawa, H., T.-J. Wang, T. T. Ishii (2002), Emergence and Drastic Breakdown of
403 a Twisted Flux Rope to Trigger Strong Solar Flares in NOAA Active Region 9026,
404 *Astrophys. J.*, *572*, 598, doi: 10.1086/340305.
- 405 Kundu, M. R., A. Nindos, J.-P. Raulin, K. Shibasaki, S. M. White, N. Nitta, K. Shibata,
406 M. Shimojo (1999), A Microwave Study of Coronal Ejecta, *Astrophys. J.*, *520*, 391, doi:
407 10.1086/307454.
- 408 Lepping, R. P., D. B. Berdichevsky, A. Szabo, C. Arqueros, A. J. Lazarus (2003), Profile
409 of an Average Magnetic Cloud at 1 au for the Quiet Solar Phase: Wind Observations,
410 *Sol. Phys.*, *212*, 425.
- 411 Liu, Y. & K. Hayashi (2006), The 2003 October-November Fast Halo Coronal Mass Ejec-
412 tions and the Large-Scale Magnetic Field Structures, *Astrophys. J.*, *640*, 1135, doi:

10.1086/500290.

Liu, Y. (2007), Halo Coronal Mass Ejections and Configuration of the Ambient Magnetic Fields, *Astrophys. J.*, *654*, L171, doi: 10.1086/511385.

López Fuentes, M. C., P. Démoulin, C. H. Mandrini, A. A. Pevtsov, L. van Driel-Gesztelyi (2003), Magnetic twist and writhe of active regions. On the origin of deformed flux tubes, *A&A*, *397*, 305, doi: 10.1051/0004-6361:20021487.

Low, B. C., J. R. Hundhausen, J. R. (1995), Magnetostatic structures of the solar corona. 2: The magnetic topology of quiescent prominences, *Astrophys. J.*, *443*, 818, doi: 10.1086/175572.

Manoharan, P. K., N. Gopalswamy, S. Yashiro, A. Lara, G. Michalek, R. A. Howard (2004), Influence of Coronal Mass Ejection Interaction on Propagation of Interplanetary Shocks, *J. Geophys. Res.*, *109*, A06109, doi: 10.1029/2003JA010300.

Martin, Sara F. (1973), The Evolution of Prominences and Their Relationship to Active Centers, *Sol. Phys.*, *31*, 3, doi: 10.1007/BF00156070.

Matsumoto, H., I. Nagano, R. R. Anderson, H. Kojima, K. Hashimoto, M. Tsutsui, T. Okada, I. Kimura, Y. Omura, and M. Okada (1994), Plasma wave observations with GEOTAIL spacecraft, *J. Geomag. Geoelectr.*, *46*, 59.

Mukai, T., S. Machida, Y. Saito, M. Hirahara, T. Terasawa, N. Kaya, T. Obara, M. Ejiri, and A. Nishida (1994), The low energy particle (LEP) experiment onboard the GEOTAIL satellite, *J. Geomagn. Geoelectr.*, *46*, 669.

Munro, R. H., J. T. Gosling, E. Hildner, R. M. MacQueen, A. I. Poland, and C. L. Ross (1979), The association of coronal mass ejection transients with other forms of solar activity, *Sol. Phys.*, *61*, 201.

- 436 Nagashima, K., H. Isobe, T. Yokoyama, T. T. Ishii, T. J. Okamoto, K. Shibata (2007),
437 Triggering Mechanism for the Filament Eruption on 2005 September 13 in Active Region
438 NOAA 10808, *Astrophys. J.*, *668*, 533, doi: 10.1086/521139.
- 439 Rust, D. M. (1994), Spawning and shedding helical magnetic fields in the solar atmosphere,
440 *Geophys. Res. Lett.*, *21*, 241.
- 441 Saito, T., Y. Kozuka, S. Tsuneta, S. Minami (1994), Rotational reversing model and
442 triple dipole model as substantiated by Yohkoh SXT data, in *Proc. Int. Symp. on the*
443 *Yohkoh Scientific Results, X-Ray Solar Physics from Yohkoh*, edited by Y. Uchida, T.
444 Watanabe, K. Shibata, & H. S. Hudson, pp. 211, Universal Academy Press, Tokyo.
- 445 Saito, Takao, K. Shibata, K. P. Dere, S. Numazawa (2000), Non-Radial Unipolar Coronal
446 Streamers in Manetically High Latitudes and Radial Bipolar Streamers at the Magnetic
447 Equator of the Sun, *Adv. Space Res.*, *26*, 807.
- 448 Scherrer, P. H., et al. (1995), The Solar Oscillations Investigation – Michelson Doppler
449 Imager, *Sol. Phys.*, *162*, 129, doi: 10.1007/BF00733429.
- 450 Sheeley, N. R., Jr., J. D. Bohlin, G. E. Brueckner, J. D. Purcell, V. Scherrer, R. Tousey
451 (1975a), XUV Observations of Coronal Magnetic Fields, *Sol. Phys.*, *40*, 103.
- 452 Sheeley, N. R., Jr., J. D. Bohlin, G. E. Brueckner, J. D. Purcell, V. E. Scherrer, R. Tousey
453 (1975b), The Reconnection of Magnetic Field Lines in the Solar Corona, *Astrophys. J.*,
454 *196*, 129.
- 455 Sheeley, N. R., Jr., J. W. Harvey, W. C. Feldman (1976), Coronal holes, solar wind
456 streams, and recurrent geomagnetic disturbances - 1973-1976, *Sol. Phys.*, *49*, 271.
- 457 Shibata, K., N. Nitta, R. Matsumoto, T. Tajima, T. Yokoyama, T. Hirayama, H. Hudson
458 (1994a), Two Types of Interaction Between Emerging Flux and Coronal Magnetic Field,

in *Proc. Int. Symp. on the Yohkoh Scientific Results, X-Ray Solar Physics from Yohkoh*,
edited by Y. Uchida, T. Watanabe, K. Shibata, & H. S. Hudson, pp. 29, Universal
Academy Press, Tokyo.

Shibata, K., N. Nitta, K. T. Strong, R. Matsumoto, T. Yokoyama, T. Hirayama, H.
Hudson, Y. Ogawara (1994b), A Gigantic Coronal Jet Ejected from a Compact Active
Region in a Coronal Hole, *Astrophys. J.*, *431*, L51, doi: 10.1086/187470.

Shibata, K., et al. (2007), Chromospheric Anemone Jets as Evidence of Ubiquitous Re-
connection, *Science*, *318*, 1591, doi: 10.1126/science.1146708.

Takahashi, Ta., T. Saito, K. Shibata, Y. Kozuka, S. Minami, Y. Mori (1994), Structure of
the Soft X-Ray Corona and its Effect to the Earth Quadrupole Type and Sea Anemone
Type, in *Proc. Int. Symp. on the Yohkoh Scientific Results, X-Ray Solar Physics from
Yohkoh*, edited by Y. Uchida, T. Watanabe, K. Shibata, & H. S. Hudson, pp. 305,
Universal Academy Press, Tokyo.

Terasawa, T., et al. (2005), Determination of shock parameters for the very fast
interplanetary shock on 29 October 2003, *J. Geophys. Res.*, *110*, A09S12, doi:
10.1029/2004JA010941.

Tian, L., D. Alexander, Y. Liu, J. Yang (2005), Magnetic Twist and Writhe of δ Active
Regions, *Sol. Phys.*, *229*, 63, doi: 10.1007/s11207-005-3524-x.

Tokumar, M., M. Kojima, K. Fujiki, A. Yokobe (2000), Three-Dimensional Propagation
of Interplanetary Disturbances Detected with Radio Scintillation Measurements at 327
MHz, *J. Geophys. Res.*, *105*(A5), 10435, doi: 10.1029/2000JA900001.

Tokumar, M., M. Kojima, K. Fujiki, M. Yamashita, A. Yokobe (2003), Toroidal-Shaped
Interplanetary Disturbance Associated with the Halo Coronal Mass Ejection Event on

- 14 July 2000, *J. Geophys. Res.*, *108*(A5), 1220, doi: 10.1029/2002JA009574.
- Tokumaru, M., M. Kojima, K. Fujiki, M. Yamashita, D. Baba (2005), Interplanetary Consequences Caused by the Extremely Intense Solar Activity During October-November 2003, *J. Geophys. Res.*, *110*, A01109, doi: 10.1029/2004JA010656.
- Tousey, R., et al. (1973), A Preliminary Study of the Extreme Ultraviolet Spectroheliograms from Skylab, *Sol. Phys.*, *33*, 265, doi: 10.1007/BF00152418.
- Verma, V. K. (1998), On the Origin of Solar Coronal Mass Ejections, *J. Ind. Geophys. Union*, *2*, 65.
- Vourlidas, A., T. S. Bastian, N. Nitta, M. J. Aschwanden (1996), Joint Radio and Soft X-Ray Imaging of an ‘Anemone’ Active Region, *Sol. Phys.*, *163*, 99, doi: 10.1007/BF00165459.
- Wang, Y.-M. (1998), Network Activity and the Evaporative Formation of Polar Plumes, *Astrophys. J.*, *501*, L145, doi: 10.1086/311445.
- Wang, Y.-M, X. Xue, C. Shen, P. Ye, S. Wang, J. Zhang (2006), Impact of Major Coronal Mass Ejections on Geospace during 2005 September 7-13, *Astrophys. J.*, *646*, 625, doi: 10.1086/504676.
- Yashiro, S., N. Gopalswamy, G. Michalek, O. C. St. Cyr, S. P. Plunkett, N. B. Rich, R. A. Howard (2004), A Catalog of White Light Coronal Mass Ejections Observed by the SOHO Spacecraft, *J. Geophys. Res.*, *109*, A07105, doi: 10.1029/2003JA010282.
- Yokoyama, T., & K. Shibata (1995), Magnetic Reconnection as the Origin of X-Ray Jets and H α Surges on the Sun, *Nature*, *375*, 42, doi: 10.1038/375042a0.
- Yokoyama, T., & K. Shibata (1996), Numerical Simulation of Solar Coronal X-Ray Jets Based on the Magnetic Reconnection Model, *PASJ*, *48*, 353.

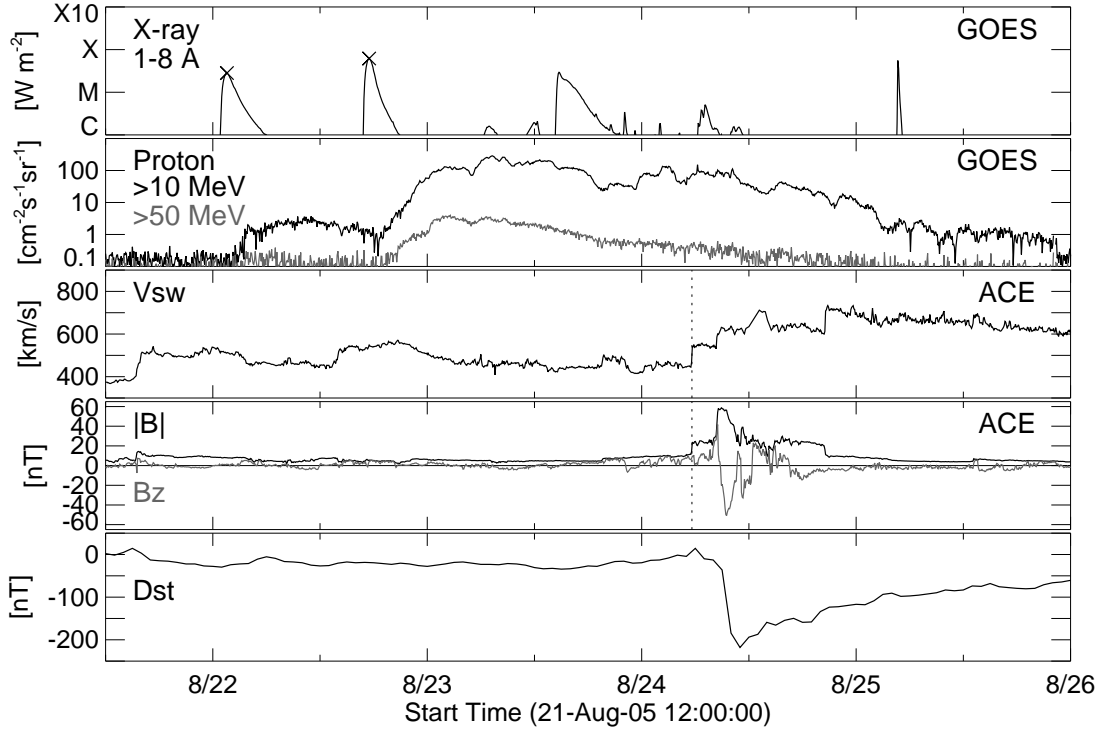


Figure 1. Overview of the geomagnetic storm that occurred on 24 August 2005, and the related solar-terrestrial events. *From top to bottom:* SXR flux in the *GOES* 1.0 - 8.0 Å channel, proton fluxes in >10 MeV (black line) and >50 MeV (gray line) channels obtained with *GOES*, bulk velocity of solar wind V_{sw} measured with *ACE*, total magnetic field strength $|B|$ (black line) and Z-component of the magnetic field B_z (gray line) measured with *ACE*, and Dst index produced by the Kyoto University.

Zhang, J., et al. (2007), Solar and interplanetary sources of major geomagnetic storms ($Dst \leq -100$ nT) during 1996–2005, *J. Geophys. Res.*, 112, A10102, doi: 10.1029/2007JA012321.

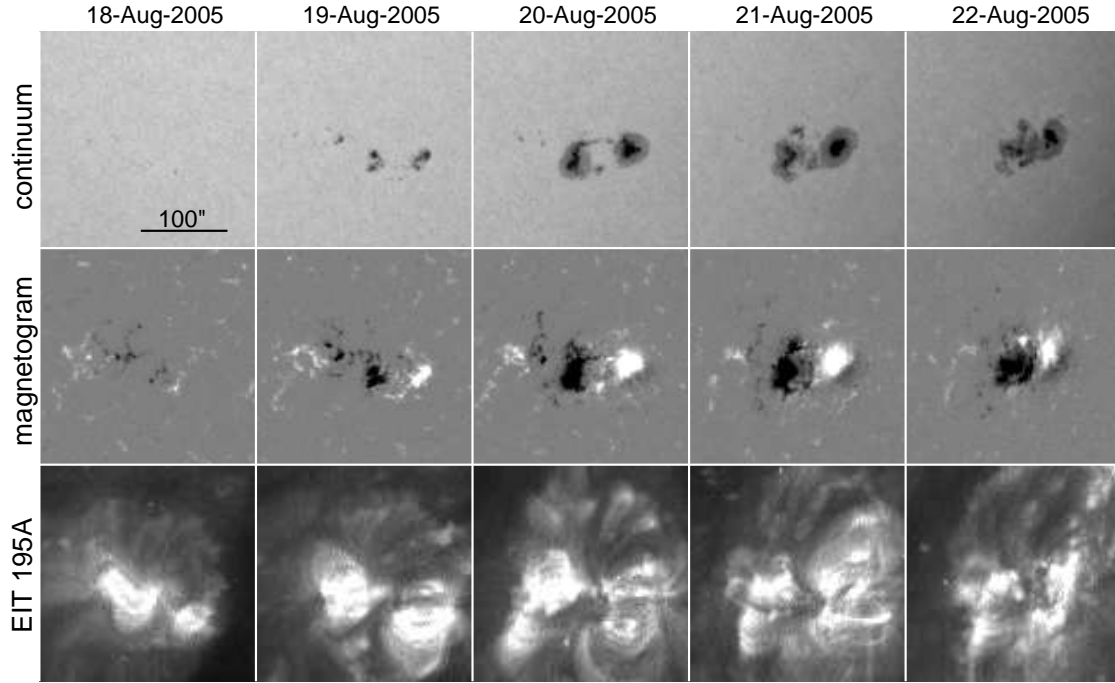


Figure 2. Temporal evolution of the AR. The top and the middle panels show the continuum images and the magnetograms observed with *SOHO*/MDI, respectively. The bottom panel shows the EUV images obtained with *SOHO*/EIT. Each image was taken at about 00:00 UT of the day. Solar north is up, and west is to the right.

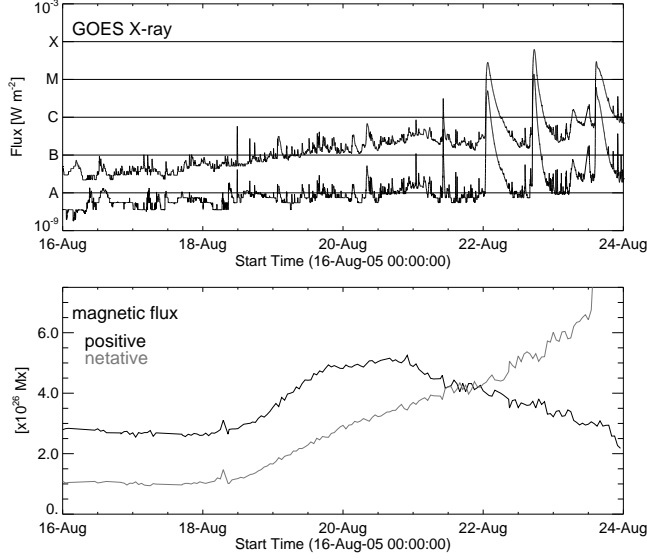


Figure 3. Time profiles of SXR flux and magnetic fluxes. *Top:* SXR flux in the *GOES* 1.0 - 8.0 Å (upper) and 0.5 - 4.0 Å (lower) channels. *Bottom:* Magnetic flux of the AR observed with *SOHO*/MDI. The calculated area is $400'' \times 400''$ centered on the middle of the AR, and is as wide as it covers the whole AR. The time profile of the negative magnetic flux is multiplied by -1 .

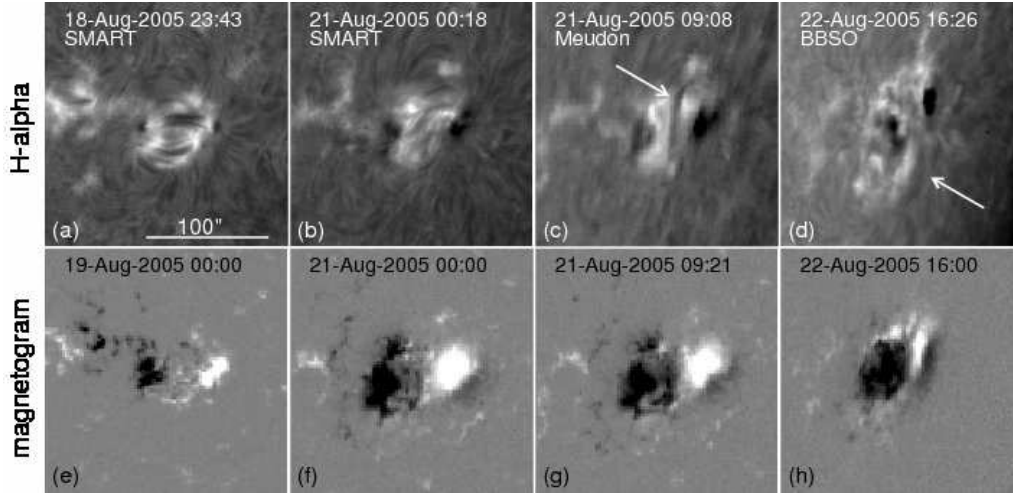


Figure 4. *Top:* $H\alpha$ images. (a) and (b) were obtained with SMART at Hida Observatory, Kyoto University. (c) and (d) were obtained at Observatoire de Paris, Section de Meudon and Big Bear Solar Observatory, respectively. *Bottom:* Magnetograms taken with *SOHO*/MDI.

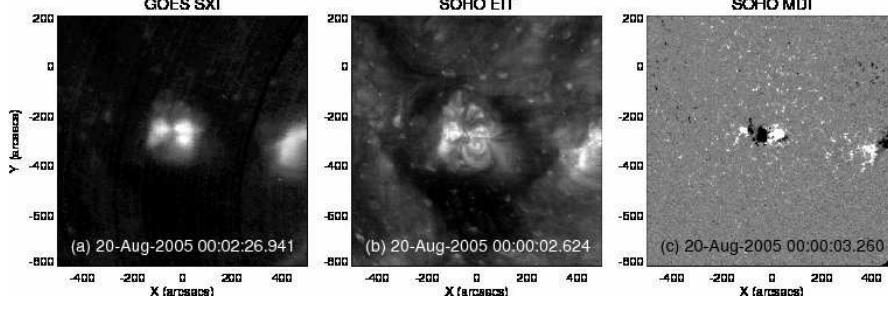


Figure 5. Coronal feature of AR 10798. (a): A SXR image obtained with *GOES*/SXI. (b): An EUV (195Å) image obtained with *SOHO*/EIT. The bright region near the center of the image is the AR. The surrounding dark region is a CH. (c): A magnetogram taken with *SOHO*/MDI.

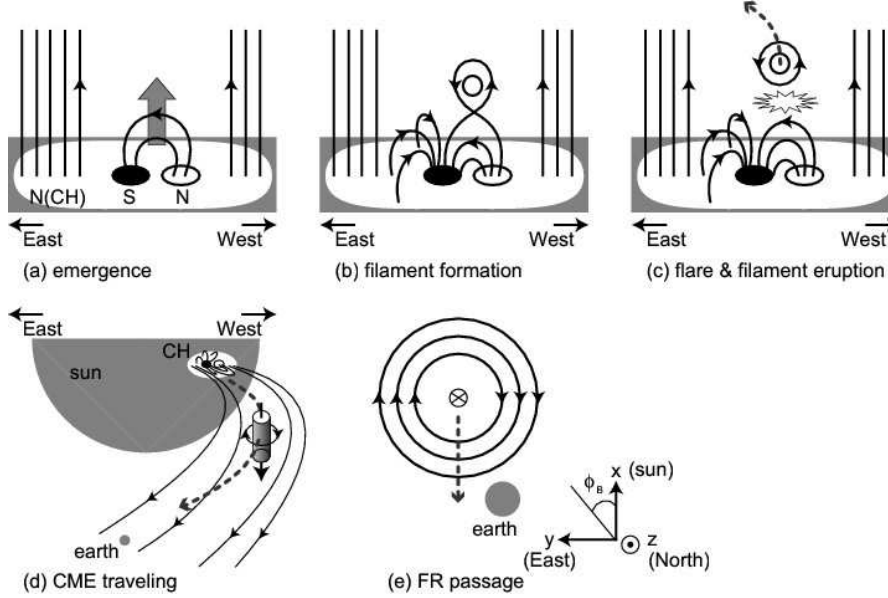


Figure 6. Schematic cartoon of AR 10798 and related flares/CMEs. (a) A magnetic flux newly emerges within a CH. (b) An anemone structure is generated, and an $H\alpha$ filament is also formed above the emerged flux. (c) A magnetic reconnection occurs beneath the filament, which causes the filament eruption. The ejected plasma is bent eastward by the surrounding magnetic field with positive magnetic polarity. (d) The ejecta becomes a magnetic cloud (shown as a cylinder) that have a southward axial magnetic field and is approaching to Earth. (e) Passage of a FR and the variation of the azimuthal angle of the magnetic field ϕ_B . When a FR passes the east of the earth, ϕ_B evolves 90 – 180 – 270 (–90) degree.

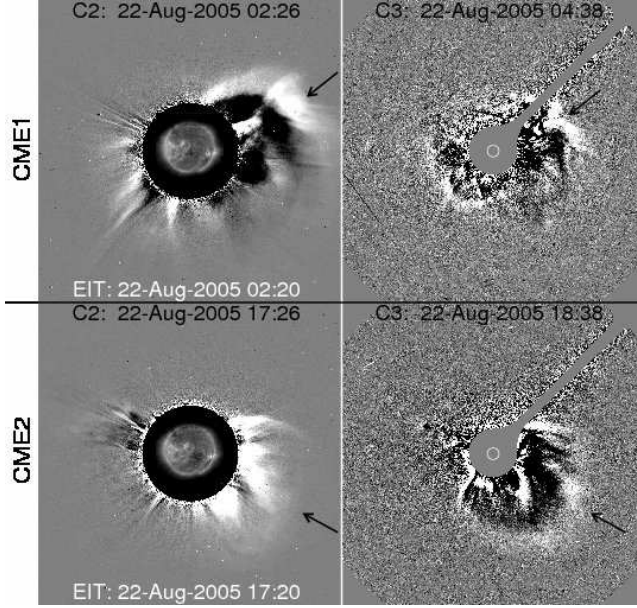


Figure 7. White-light CME images obtained with *SOHO*/LASCO. The left two panels show C2 running difference images for CME1/CME2 overlaid with EUV images obtained with *SOHO*/EIT (195Å). The right two panels show C3 running difference images. The arrows roughly point the main part of CMEs.

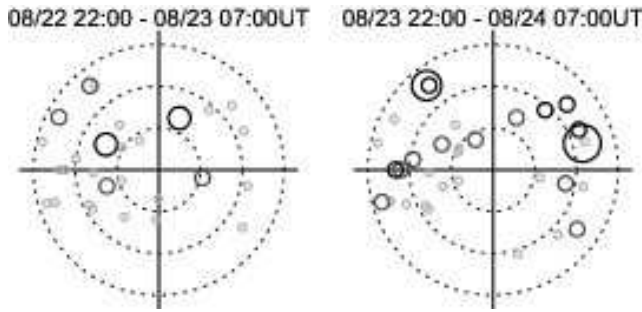


Figure 8. Daily (Japanese daytime) sky projection maps of g-values obtained with IPS observations at STEL Nagoya University. In each map, the center corresponds to the Sun center, and the dotted cocentric circles are constant radii contours from the Sun drawn at 0.3, 0.6, and 0.9 AU. Solid circles indicate the points of the closest approach to the Sun (P-points) on the line-of-sight where g-value data were obtained (P-point approximation). Dark gray and black circles represent the locations where the g-values are larger than 1.5 and 2.0, respectively.

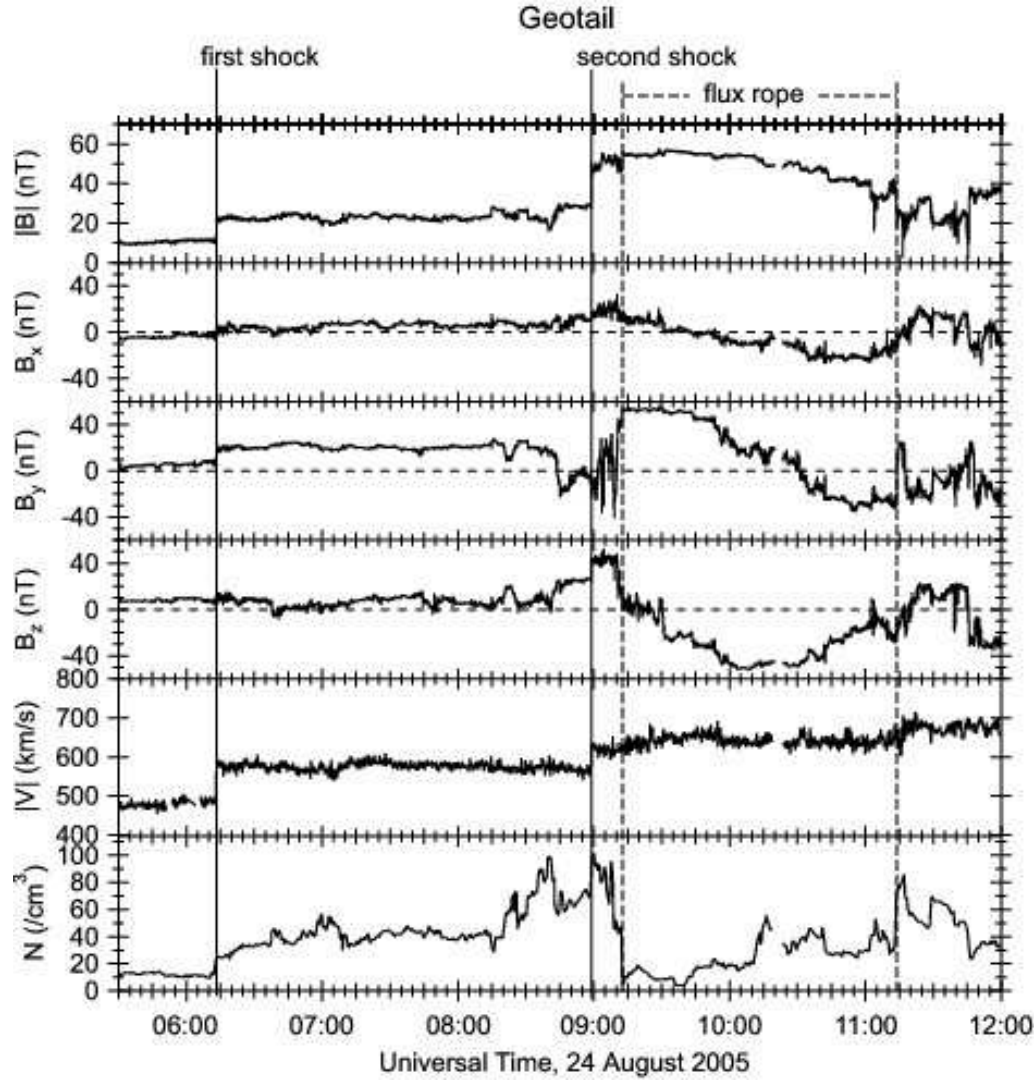


Figure 9. *Geotail* observation of the interplanetary disturbance on 24 August 2005. *From top to bottom:* magnitude and X-, Y-, and Z- components in GSE coordinate of the magnetic field (MGF experiment), ion velocity (LEP/SWI experiment), and electron density (PWI/SFA). The vertical solid lines show the shocks (the first and the second shocks). The vertical dashed lines show the flux rope.